AADE-12-FTCE-37

# Geomechanical Wellbore Stability Analysis for Deviated Wells based on Vertical Exploration Data

Steven Hilgedick and Runar Nygaard, Missouri University of Science and Technology, Svein Hellvik and Espen Hoel, Lundin Petroleum Norway AS



## Abstract

As part of the deviated and horizontal production wells design in the recent discovery in the North Sea, wellbore stability analysis was conducted. The analysis requires integration of well log analysis; rock mechanical testing for rock deformation properties and rock strength parameters, well test analysis for in-situ stress determination, and application of failure criteria. This work details a practical methodology for both planning your data collection program during exploratory drilling to aid in developing a geomechanical wellbore model and the development and use of such a model in determining wellbore stability criteria for inclined wellbores. First step of a geomechanical model is to determine in-situ stresses based on interpretation of leak off, extended leak off and mini-frac tests for determining minimum and maximum horizontal stress magnitude as well as well log analysis yielding stress orientations. Then the geomechanical rock model which includes the deformation and strength properties for all formations along the well path was developed. Rock strength calculations are based on log correlations relating well log analysis to rock strength for different lithologies. Rock deformation properties were determined based on acoustic wave velocities. The wellbore stability analysis was then applied for the directional well path and mud weights were selected. Breakout in the first deviated wellbore in the field caused by mudweight selected below the recommended mud weight from this study verified the geomechanical model. Selecting an appropriate data collection program in the exploratory drilling process proved invaluable when conducting the analysis.

## Introduction

### *In-situ stress magnitude*

This methodology is based off of the assumption that the vertical stress ($\sigma_v$) is one of the principle in-situ stresses ($\sigma_1$, $\sigma_2$, $\sigma_3$) and the other two are the minimum and maximum horizontal stresses ($\sigma_h$ and $\sigma_H$). This is a safe assumption for areas with little tectonic activity. It is important to consider that in areas with strong tectonic forces or near complex geological structures, such as near a salt dome, that the stress field can be drastically different [1].

Vertical stress or overburden may be calculated from well log analysis. In areas with low tectonic activity the vertical stress can be calculated by integrating the density log over the vertical depth using Equation 1 onshore or Equation 2 for offshore wells [6]. Here density ($\rho$) from logs is used to calculate $\sigma_v$ through the depth of interest ($z$) based on water density ($\rho_w$) and the water depth ($z_w$).

$$\sigma_v = \int_0^z \rho(z) g \, dz \tag{1}$$

$$\sigma_v = \rho_w g z_w + \int_0^z \rho(z) g \, dz \tag{2}$$

For shallow zones, where density logs are not available, a range of 1.8-2.0 g/cc can be used related to a porosity of 38-50% and a mineral density of 2.6 g/cc. Geological history must also be taken into account in areas such as off-shore Norway where shallow bulk densities above 2.0 g/cc have been recorded as a result of ice loading [1].

Horizontal stress magnitudes must be determined from the interpretation of extended leak off (XLOT) and mini-frac tests. Standard leak off tests can only show a fracture initiation point and therefore cannot serve in calculating a true $\sigma_h$ value. In a XLOT or a mini-frac test pumping is continued past the fracture breakdown pressure until stable fracture growth is achieved [2]. This creates a fracture that reaches beyond near wellbore stresses into the far-field virgin stresses. Pumping is then stopped and shut-in decline pressure is measured over a period of time. For best results this operation should be performed multiple times.

Shut-in pressure decline analysis from these tests can be used to determine $\sigma_h$. Several methods exist for determining fracture closure pressure including pressure during the shut in phase plotted as pressure vs. time, the square root of time, log of time, or log of pressure vs. log of time [3, 4, and 5]. In these the initial shut in pressure is the absolute maximum value of $\sigma_h$, however the fracture closure pressure is considered to be the best estimate [6]. The ISIP is the pressure recorded immediately after pumping has stopped and the well is shut-in. After this the decline approaches a linear fit as the fracture is still held open. The fracture closure pressure can be seen on the shut-in phase plot as where the pressure decline deviates

from this linear trend. The deviation can be an increase or decrease in the rate of change depending on rock properties and geometry and fluid properties.

The maximum horizontal stress magnitude was solved based on impermeable fracture modeling of XLOT data. Equation 3 shows the fracture initiation pressure ($P_{frac}$) for an impermeable formation with $\sigma_h$ as the minimum principle stress and $\sigma_H$ as the intermediate principle stress in a vertical well [6].

$$P_{frac} = 3\sigma_h - \sigma_H - P_p + T_0 \quad (3)$$

### *In-situ stress orientation*

Determination of horizontal principle stress orientations requires the analysis of failure around the wellbore. Tensile failure or fractures which are formed along the wellbore while drilling occur along the orientation of $\sigma_H$. Shear failure known as breakouts occur along the orientation of $\sigma_h$. Analysis of these failures requires either caliper logs or image logs based on acoustic borehole imaging. Caliper logs have traditionally been used as the arms will seat themselves in line with the breakouts and show larger diameter measurements from those arms [7]. Caliper logs do however show some difficulty in consistently differentiating between breakouts and keyseating [8].

The use of borehole imaging logs alleviates some of the uncertainty with regards to key seating vs. failure induced wellbore elongation. Image logs also make it possible to identify fractures and differentiate between naturally occurring fractures and drilling induced fractures. Borehole image logs based on resistivity are made up of many electrodes attached to 4 to 6 arms that run against the formation. These logs provide resistivity for a very shallow depth of investigation making it possible to identify bedding planes, natural fractures, and drilling induced fractures [1]. Acoustic imaging logs on the other hand measure acoustic wave travel time of waves reflecting off of the borehole wall. This makes them ideal for measuring breakout orientation from wellbore elongation however they cannot typically determine fracture orientation as fractures do not create large changes in borehole radius or reflectivity [1].

### *Mechanical Model Development*

Rock strength and deformation properties define the way the materials react to stresses applied to them. Wellbore stability analysis applies stresses near the wellbore to these mechanical properties. These properties can be determined through mechanical tests which yield static strength and deformation properties or non-destructive tests (well logs) which yield dynamic material properties. Static strength and deformation properties are considered the most representative of actual material behavior however these require cores taken from the formation for testing and only represent the material properties at that specific location. Dynamic material properties on the other hand can be calculated from well logs and provide a complete view of material characteristics along the entire wellbore.

Static rock strength and deformation properties are determined through triaxial tests run on core samples taken from vertical reference wells. Strength properties can be determined by running multiple triaxial tests at varying levels of confining stress the peak axial stress from each test can be plotted against the confining stress for that test. A linear trend from this plot shows the unconfined compressive strength (UCS) as the intercept of this line with the vertical axis. The slope of this line ($\gamma$) can be related to the failure angle ($\beta$) for Mohr-Coulomb failure criteria through equation 4 and equation 5 where $\varphi$ is the friction angle [9].

$$\sin\varphi = \frac{\tan\gamma - 1}{\tan\gamma + 1} \quad (4)$$

$$\beta = \frac{\pi}{4} + \frac{\varphi}{2} \quad (5)$$

By recording radial and axial strain during triaxial testing the static deformation properties can be determined. The static Young's modulus ($E_s$) can be calculated from axial stress ($\sigma_x$) and axial strain ($\varepsilon_x$) in equation 6. The static Poisson's ratio ($\nu_d$) is calculated from axial and radial strain ($\varepsilon_y$) using equation 7.

$$E_s = \frac{\sigma_x}{\varepsilon_x} \quad (6)$$

$$\nu_d = \frac{\varepsilon_y}{\varepsilon_x} \quad (7)$$

Dynamic strength and deformation properties can be calculated from acoustic velocity, bulk density logs, and lithology. Several methods exist for lithology determination [10]. For this field lithology was divided into carbonates and silisticlastic rocks and the amount of clay minerals was derived from gamma ray logs since the regional lithology is well known [8]. This lithology was then applied to the regional rock strength correlation given in equation 8 [11]. In equation 8 UCS is the unconfined compressive strength in MPa. k1, k2, k3 are constants based on lithology and $\Delta t_c$ is compressive travel time in µsec/ft.

$$UCS = \left(\frac{1.00}{k_1(\Delta t_c - k_2)}\right) + k_3 \quad (8)$$

Failure angle was also calculated based on lithology. First $\gamma$, the Mohr-Coulomb relationship between minimum and maximum principle stresses at failure, was calculated from equation 9 for sandstone and equation 10 for shale [12]. The value was then related to $\beta$ using equation 4 and equation 5.

$$\gamma = 3.9 \ln(UCS) + 60 \quad (9)$$

$$\gamma = 7.2 \ln(UCS) + 39 \quad (10)$$

Dynamic Poisson's ratio and Young's modulus can be calculated from P- (Compressional) and S- (Shear) wave velocity logs (acoustic) and density logs. Equation 11 calculates the dynamic Poisson's ratio ($\nu_d$) from the relationship between the P- wave velocity ($V_P$) and S- wave velocity ($V_S$).

$$\nu_d = \frac{V_P^2 - 2V_S^2}{2(V_P^2 - V_S^2)} \quad (11)$$

The dynamic Elastic Young's modulus can be calculated from S- wave velocity and rock density (ρ) logs using equation 12.

$$E_d = 2\rho V_S^2(1 + \nu_d) \quad (12)$$

Young's modulus is in GPa, ρ is in (g/cm3). Since dynamic properties are determined from elastic deformation by acoustic waves it is questionable how representative the dynamic properties are for studying geo-mechanical problems such as wellbore stability. Therefore correlations between dynamic and static deformation properties from triaxial testing results were used to determine the static Young's modulus and Poisons ratio.

## Stability Analysis

Once the Geomechanical model from vertical reference well data is completed then mechanical failure can be applied for wellbore stability analysis. For failure criteria to be applied the state of stress around the wellbore must be determined. For deviated wells the principle in-situ stresses usually do not align with the wellbore orientation. For these cases complex stress transformations must be completed to determine the principle stresses in the wellbore wall.

Fundamentally it is known that one of the principle stresses in the wellbore wall is equal to the effective radial stress ($\sigma_{rr}$) shown in equation 13. The other principle stresses exist in a plain tangential to the wellbore wall, orthogonal to each other at any orientation around the wellbore wall. The tangential stresses ($\sigma_{tmax}$ & $\sigma_{tmin}$) can be calculated using the Kirsh equation applied to an arbitrary wellbore orientation in equation 14 and equation 15 where $\sigma_{zz}$, $\sigma_{\theta\theta}$, and $\tau_{\theta z}$ are the transformed from in-situ stresses and have been included in Appendix A.

$$\sigma_{rr} = P_w - P_P \quad (13)$$

$$\sigma_{tmax} = \frac{1}{2}(\sigma_z + \sigma_\theta + \sqrt{(\sigma_z - \sigma_\theta)^2 + 4\tau_{\theta z}^2}) - P_P \quad (14)$$

$$\sigma_{tmin} = \frac{1}{2}(\sigma_z + \sigma_\theta - \sqrt{(\sigma_z - \sigma_\theta)^2 + 4\tau_{\theta z}^2}) - P_P \quad (15)$$

Once these stresses have been determined they are arranged based on magnitude and set to equal the principle stresses $\sigma_1$, $\sigma_2$, and $\sigma_3$ so that failure criteria can be applied. There are several different failure criteria which can be used. For analysis of breakouts due to shear failure Mohr-Coulomb criterion has been applied [13]. For determination of when shear failure will occur the variation of Mohr-Coulomb failure stated in equation 16 can be applied. In order to determine the principle stresses in which shear failure will occur $P_w$ must be varied to determine the highest allowable mudweight to counteract the In-situ stresses and satisfy equation 16.

$$\sigma_1' - \tan\gamma\, \sigma_3' > UCS \quad (16)$$

Tensile failure calculations are based on equation 17. This states that rocks will fail in tension when the minimum principle stress is less than the tensile strength ($T_0$) which is numerically negative [9]. It is important to note that rocks have very little strength in tension and many rocks have pre-existing fractures which can reduce their tensile strength to zero.

$$\sigma_3' < T_0 \quad (17)$$

## Results

When planning the first deviated well in the discovery data from nearby exploratory wells was used for developing the geomechanical model. Wellbore image logs were used to determine maximum horizontal stress orientation shown in figure 1 by drilling induced fractures at a 90-120o and 270-290o azimuth. XLOT and mini-frac data was taken from exploratory wells in this field. Figure 2 below shows the mini-frac data from one of the reference wells where multiple pumping cycles were completed to verify the fracture closure pressure. The stress profiles calculated from these test are included in the mudweight window plots for wellbore stability analysis along the surveyed wellpath along with the pore pressure profile used and the vertical stress calculated from density logs.

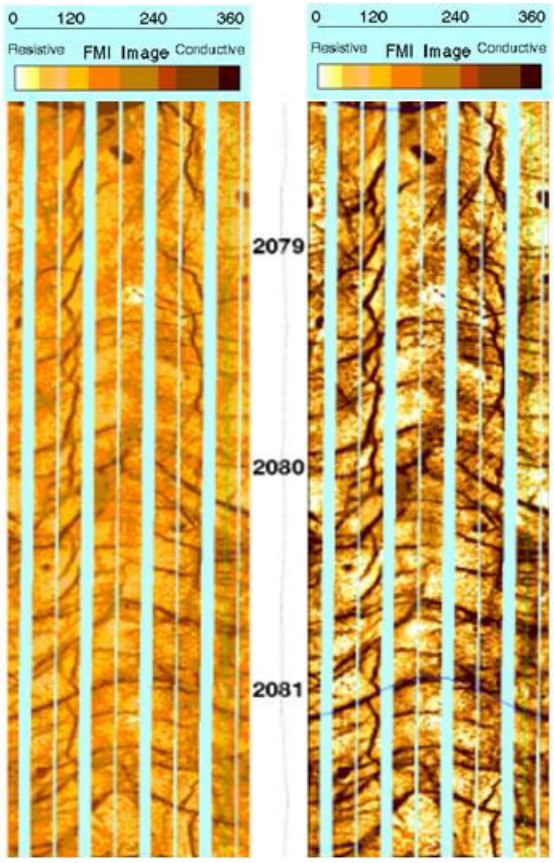


Figure 1. Image logs showing drilling induced fractures in the maximum horizontal stress orientation.

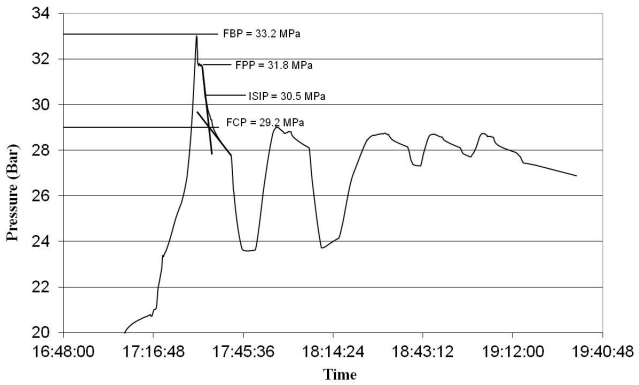


Figure 2. Mini-frac data from a vertical reference well.

Figure 3 shows the rock strength calculated for the geomechanical model developed for this field. A general lithological overview of the formations in this interval is also included. Further details regarding the geomechanical model results are included in Hilgedick 2012 [14].

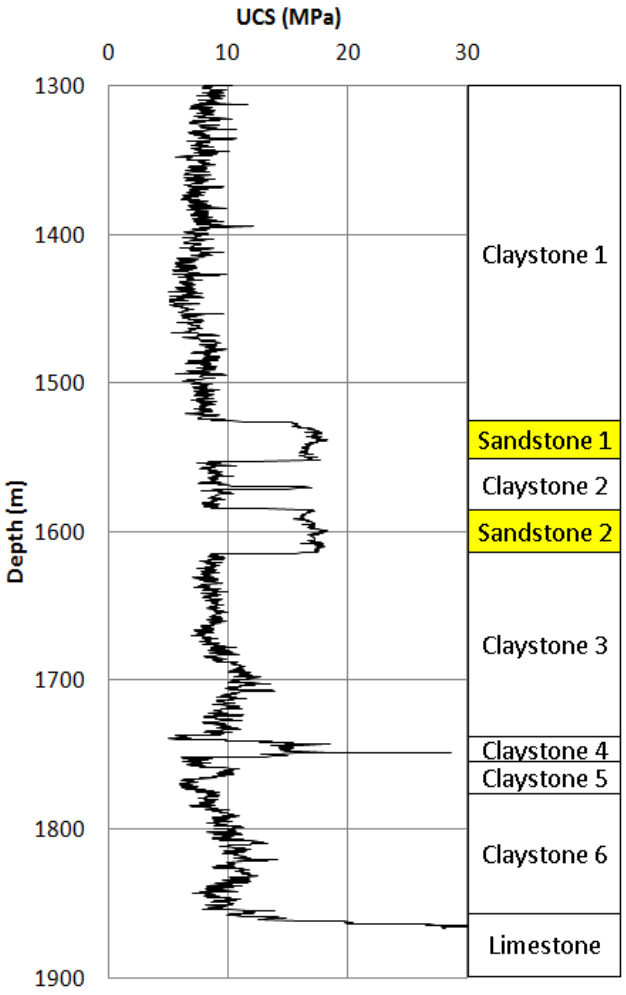


Figure 3. Strength plot and lithological overview of zone of interest from geomechanical model.

Due to the forces around the wellbore while drilling the safest wellbore azimuth is always parallel to the minimum horizontal stress orientation. Likewise the least stable wellbore azimuth falls in the orientation of the maximum horizontal stress orientation. Overall wellbore stability analysis was completed for this field which forecasts the mudweight window at any inclination for both extremes along the minimum and maximum horizontal stress orientations. Figure 4 through Figure 6 show this analysis for the weaker formations which govern the mudweight selection for this well section. Any wellbore orientation between the minimum and maximum horizontal stress orientations will result in an acceptable mudweight between forecast values in those orientations.

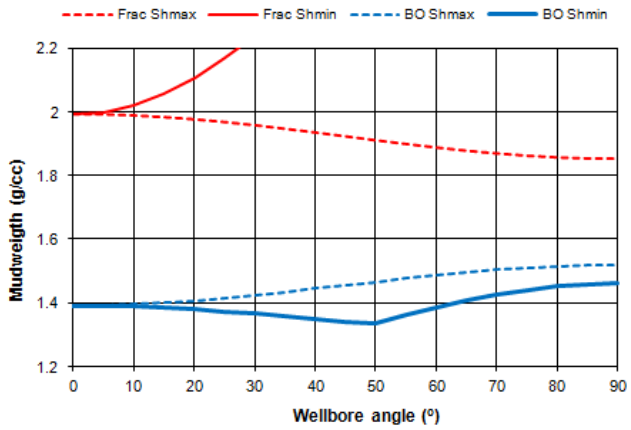


Figure 4. Forecast mudweight window for claystone 1 interval at any inclination along the minimum and maximum horizontal stress orientations.

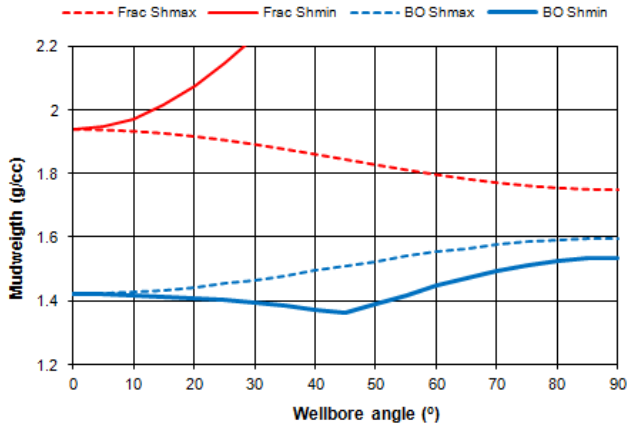


Figure 5. Forecast mudweight window for claystone 3 interval at any inclination along the minimum and maximum horizontal stress orientations.

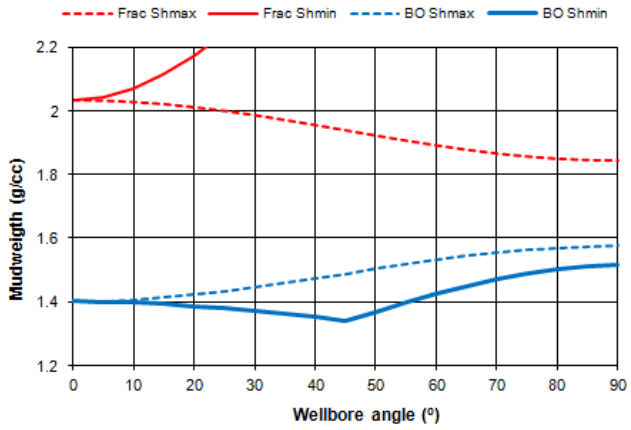


Figure 6. Forecast mudweight window for claystone 5 interval at any inclination along the minimum and maximum horizontal stress orientations.

A wellbore stability analysis was completed based on the specific inclination and azimuth along the entire well path. This analysis determined overall minimum mudweight values to avoid wellbore breakouts as well as maximum mudweight of to avoid fractures assuming intact rock without pre-existing fractures. This mudweight window can be seen in Figure 7. Plots of in-situ stresses were also included along with fracture pressure based on LOT and XLOT data from reference wells. From this it can be seen that based on the geomechanical model the minimum allowable mudweight to avoid breakouts is 1.43 sg without considerations for pressure drop while tripping and the maximum mudweight to avoid fractures of 1.8 sg.

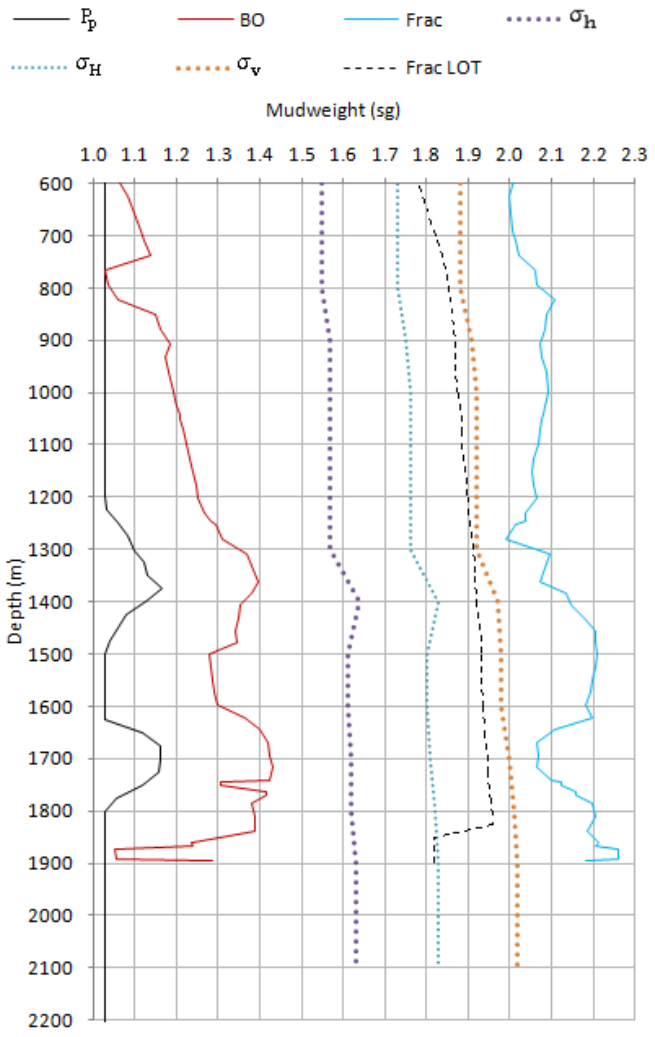


Figure 7. Mudweight window forecast from geomechanical wellbore stability analysis.

The study well was drilled in the section of interest at an azimuth 36° from the minimum horizontal stress orientation and inclination of 34°. This section was drilled to 1879.4 mTVD with a mudweight of 1.4 sg. This mudweight was selected with other drilling consideration beyond wellbore stability while drilling. While drilling this well section multiple areas of breakouts were observed and excessive cavings form the weak shale horizons were reported which corresponded to the weaker formation sections included in Figure 4 through Figure 6.

## Conclusions

- Analysis of the breakouts seen in the study well demonstrates the validity of the wellbore stability analysis of this well.
- Concise geomechanical models can be developed based on data from vertical exploratory wells. This model shows that the assumptions used in this methodology provide an accurate model of the stresses in and mechanical properties of the rock.
- The use of Mohr-Coulomb failure criterion alone provides adequate failure analysis for wellbore stability calculation in the lithologies present in the study well.

## Acknowledgments

The authors would like to thank Lundin Norway AS for funding this research project at Missouri S&T.

## References

1. Fjaer, E., R.M. Holt, P. Horsrud, A.M. Raaen, and. R. Risnes. 2008. *Petroleum Related Rock Mechanics.* 2nd ed. Elsevier. Amsterdam.
2. Kunze, K.R., and R.P. Steiger. 1992. Accurate In-Situ Stress Measurements During Drilling Operations. SPE 24593. Presented at the 67th Annual Technical Conference and Exhibition, Washington DC, 4-7 October, 1992.
3. Lee, M.Y., and B.C. Haimson. 1989. Statistical Evaluation of Hydraulic Fracturing Stress Measurement Parameters. *Int. J. Rock Mech.* 26: 447-456.
4. Turnbridge, L.W. 1989. Interpretation of the Shut-In Pressure from the Rate of Pressure Decay. *Int. J. Rock Mech.* 26: 457-460.
5. Amadei, B., and O. Stephansson. 1997 *Rock Stress and its Measurement. Chapman & Hall.* London and New-York.
6. Jaeger, J.C., N.G.W. Cook, R.W. Zimmerman. 2007. *Fundamentals of Rock Mechanics.* 4th ed. Blackwell Publishing.
7. Plumb, R.A. 1985. Stress-Induced Borehole Elongation: A Comparison Between the Four Arm Dipmeter and The Borehole Televiewer in the Auburn Geothermal Well. *J. Geophys. Res.* 90: 5,513-5,521.
8. Fejerskov, M., and R.K. Bratli. 1998. Can Dipmeter Logs be used to Identify In-Situ Stress Directions in the North Sea. SPE/ISRM 47236. In *Proc. Eurock '98, Trondheim, Norway 8-10 July 1998, 151-160.* Society of Petroleum Engineers
9. Aadnoy, B.S., I. Cooper, S.Z. Miska, R.F. Mitchell, and M.L. Payne. 2009. *Advanced Drilling and Well Technology.* Society of Petroleum Engineers.
10. Bassiouni, Z. 1994. *Theory, Measurement, and Interpretation of Well Logs*. Society of Petroleum Engineers.
11. Nygaard, R., and G. Hareland. 2007. Application of Rock Strength in Drilling Evaluation. SPE 106573. Presented at the Latin American and Caribbean Petroleum Engineering Conference, Buenos Aires, Argentina, 15-18 April, 2007.
12. Hareland, G. and R. Nygaard. 2008. Calculating Unconfined Rock Strength from Drilling Data. In *Proceedings of the 1st Canada-US Rock Mechanics Symposium, Vancouver, Canada, 27–31 May 2007*, eds E.B. Eberhardt et al, 1717–1723. London: Taylor & Francis.
13. Goodman, R.E. 1989. *Introduction to Rock Mechanics.* 2nd ed. John Wiley & Sons. New York and Chichester.
14. Hilgedick, S.A. 2012. PhD Dissertation. Missouri University of Science and Technology. *In prep*.
15. Bradley, W.B. 1979. Failure of Inclined Boreholes. J. *Energy Res. Tech.* 101: 232-239.

## Appendix A

Equations for stresses around an arbitrarily oriented wellbore were first solved by Bradley (1979) [15]. To transform in-situ stresses to principle stresses around an inclined wellbore you must first define the right handed coordinate system ($x'$, $y'$, $z'$) where $x'$ is parallel to $\sigma_H$, $y'$ is parallel to $\sigma_h$, and $z'$ is parallel to $\sigma_v$ with an upward orientation. Second the right handed borehole coordinate system, (x, y, z), must be defined where the x-axis is passes through the center of the borehole and through the wellbore wall at the lowest point normal to the wellbore wall. The y-axis passes through the center of the borehole at the same location and runs horizontal through the borehole wall. The z-axis runs upward through the center axis of the borehole and i denotes the angle between the $z'$-axis and the z-axis. The angle between the $x'$-axis and the projection of the x-axis on the ($x'$, $y'$) plane is α. The transform between these coordinate systems can be described by direction cosines, where $l_{ij'}$ is the cosine of the angle between the i-axis and the j-axis. From this Equation 18 through Equation 26 can be derived.

$$l_{xx'} = \cos\alpha \cos i \quad (18)$$
$$l_{xy'} = \sin\alpha \cos i \quad (19)$$
$$l_{xz'} = -\sin i \quad (20)$$
$$l_{yx'} = -\sin\alpha \quad (21)$$
$$l_{yy'} = \cos\alpha \quad (22)$$
$$l_{yy'} = 0 \quad (23)$$
$$l_{zx'} = \cos\alpha \sin i \quad (24)$$
$$l_{zy'} = \sin\alpha \sin i \quad (25)$$
$$l_{zz'} = \cos i \quad (26)$$

From these equations the in-situ stresses $\sigma_V$, $\sigma_H$, and $\sigma_h$can be expressed in the (x, y, z) coordinate system using Equation 27 through Equation 32, where $\sigma_i^0$ is the far field stress in the i orientation.

$$\sigma_x^0 = l_{xx'}^2\sigma_H + l_{xy'}^2\sigma_h + l_{xz'}^2\sigma_V \quad (27)$$
$$\sigma_y^0 = l_{yx'}^2\sigma_H + l_{yy'}^2\sigma_h + l_{yz'}^2\sigma_V \quad (28)$$
$$\sigma_z^0 = l_{zx'}^2\sigma_H + l_{zy'}^2\sigma_h + l_{zz'}^2\sigma_V \quad (29)$$
$$\tau_{xy}^0 = l_{xx'}l_{xy'}\sigma_H + l_{xy'}l_{yy'}\sigma_h + l_{xz'}l_{yz'}\sigma_V \quad (30)$$
$$\tau_{yz}^0 = l_{yx'}l_{zx'}\sigma_H + l_{yy'}l_{zy'}\sigma_h + l_{yz'}l_{zz'}\sigma_V \quad (31)$$
$$\tau_{zx}^0 = l_{zx'}l_{xx'}\sigma_H + l_{zy'}l_{xy'}\sigma_h + l_{zz'}l_{xz'}\sigma_V \quad (32)$$

Transferring farfield stresses to stresses at the wellbore wall is best done in cylindrical polar coordinates r, theta, and z, where r is the distance from the borehole axis, theta is the angle of rotation around the wellbore from the x-axis, and z is the position along the borehole axis. Based on linear elasticity and isotropic rock properties Equation 33 to Equation 38 can be derived from plane strain conditions.

$$\sigma_r = P_w \quad (33)$$
$$\sigma_\theta = \sigma_x^0 + \sigma_y^0 - 2\left(\sigma_x^0 - \sigma_y^0\right)\cos 2\theta + 4\tau_{xy}^0 \sin 2\theta - P_w \quad (34)$$
$$\sigma_z = \sigma_x^0 - \upsilon\left[2\left(\sigma_x^0 - \sigma_y^0\right)\cos 2\theta + 4\tau_{xy}^0 \sin 2\theta\right] \quad (35)$$
$$\tau_{r\theta} = 0 \quad (36)$$
$$\tau_{\theta z} = 2\left(-\tau_{xz}^0 \sin\theta + \tau_{yz}^0 \cos\theta\right) \quad (37)$$
$$\tau_{rz} = 0 \quad (38)$$